Electronic Supplementary Information

for

Temperature-Tunable Multiple Dielectric Switch in Hybrid Rare-Earth Perovskites Regulated by Hierarchical Guest Dynamics, Lanthanide Contraction and Doping

Hui Xiao,[a,d] Lin-Yong Sheng,[a,d] Shuai Chen,[b,d] Rui-Kang Huang,*[c] Cheng-Hui Zeng,[a] Zi-Yi Du,*[a] Chun-Ting He,[a] Wei-Xiong Zhang*[b] and Xiao-Ming Chen[b]

[a]College of Chemistry and Chemical Engineering, Jiangxi Normal University, Nanchang 330022, China

[b]MOE Key Laboratory of Bioinorganic and Synthetic Chemistry, GBRCE for Functional Molecular Engineering, School of Chemistry, IGCME, Sun Yat-Sen University, Guangzhou 510275, China

[c]Graduate School of Environmental Science, Hokkaido University, Sapporo 060-0810, Japan; Research Institute for Electronic Science (RIES), Hokkaido University, Sapporo 001-0020, Japan

[d]These authors contributed equally

*Correspondence to: Zi-Yi Du, E-mail: ziyidu@gmail.com; Rui-Kang Huang, E-mail: huangrk@es.hokudai.ac.jp; Wei-Xiong Zhang, E-mail: zhangwx6@mail.sysu.edu.cn

Table S1 The phase transition temperatures T_1/T_2 (K) and thermal hystereses of **1**-**4** within a heating–cooling cycle recorded by DSC measurement

	$T_{1\text{-heating}}$	$T_{1\text{-cooling}}$	$\Delta T_{1\text{- hysteresis}}$	$T_{2\text{-heating}}$	$T_{2\text{-cooling}}$	$\Delta T_{2\text{- hysteresis}}$
1	282	278	4	-	-	-
2	283	280	3	258	245	13
3	287	283	4	229	209	20
4	285	281	4	206	180	26

Table S2 Summary of crystal data and structural refinements for **2** at three phases

Empirical formula		$C_{10}H_{28}N_8O_{18}CeRb$	
Formula weight		773.99	
T (K)	173(2)	273(2)	293(2)
Phase	**2α**	**2β**	**2γ**
Space group	$C2/m$	$R\bar{3}_m$	$F\bar{m}3_m$
a (Å)	17.067(3)	9.8698(5)	14.0164(4)
b (Å)	9.8843(18)	9.8698(5)	14.0164(4)
c (Å)	9.8724(18)	24.1798(16)	14.0164(4)
β (deg)	125.18(2)	-	-
V (Å^3)	1361.2(5)	2039.9(2)	2753.7(2)
Z	2	3	4
D_{calcd} (g cm^{-3})	1.888	1.890	1.867
μ (mm^{-1})	3.537	3.541	3.497
GOF on F^2	1.048	1.030	1.035
R_1, wR_2 $[I > 2\sigma(I)]^a$	0.1096, 0.2942	0.0550, 0.1274	0.0351, 0.1064
R_1, wR_2 (all data)	0.1425, 0.3209	0.0895, 0.1458	0.0546, 0.1228

$^aR_1 = \sum||F_o| - |F_c||/\sum|F_o|$, $wR_2 = \{\sum w[(F_o)^2 - (F_c)^2]^2/\sum w[(F_o)^2]^2\}^{1/2}$

Table S3 Summary of crystal data and structural refinements for **1**, **3** and **4**

Phase	**1α**	**1γ**	**3γ**	**4γ**
Empirical formula	$C_{10}H_{28}N_8O_{18}LaRb$		$C_{10}H_{28}N_8O_{18}NdRb$	$C_{10}H_{28}N_8O_{18}SmRb$
Formula weight	772.52		778.08	784.19
T (K)	223(2)	293(2)	293(2)	293(2)
Space group	$C2/m$	$Fm\bar{3}m$	$Fm\bar{3}m$	$Fm\bar{3}m$
a (Å)	16.776(10)	14.0679(2)	14.0073(3)	13.9697(2)
b (Å)	10.103(3)	14.0679(2)	14.0073(3)	13.9697(2)
c (Å)	9.529(5)	14.0679(2)	14.0073(3)	13.9697(2)
β (deg)	122.57(8)	-	-	-
V (Å^3)	1361.2(16)	2784.1(1)	2748.3(2)	2726.2(1)
Z	2	4	4	4
D_{calcd} (g cm^{-3})	1.886	1.843	1.881	1.911
μ (mm^{-1})	3.434	3.358	3.737	4.016
GOF on F^2	1.099	1.038	1.156	1.046
R_1, wR_2 [$I > 2\sigma(I)$][a]	0.0787, 0.2268	0.0518, 0.1279	0.0511, 0.0881	0.0487, 0.1270
R_1, wR_2 (all data)	0.0832, 0.2324	0.0727, 0.1395	0.0530, 0.0888	0.0631, 0.1393

[a] $R_1 = \sum||F_o| - |F_c||/\sum|F_o|$, $wR_2 = \{\sum w[(F_o)^2 - (F_c)^2]^2/\sum w[(F_o)^2]^2\}^{1/2}$

Table S4 Selected bond lengths (Å) for **2** at different phases

		2α at 173 K	
Ce(1)–O(2)	2.49(5)	Ce(1)–O(5)	2.54(4)
Ce(1)–O(2A)	2.59(2)	Ce(1)–O(6)	2.60(2)
Ce(1)–O(6A)	2.62(2)	Rb(2)–O(3)	2.85(3)
Rb(2)–O(1)#1	2.73(1)		
		2β at 273 K	
Ce(1)–O(3)	2.59(1)	Ce(1)–O(4)	2.605(1)
Rb(2)–O(5)	2.734(9)		
		2γ at 293 K	
Ce(1)–O(4)	2.60(5)	Ce(1)–O(5)	2.66 (5)
Rb(2)–O(3)	2.83 (2)		

Symmetry code: #1. 1/2 – *x*, 1/2 – *y*, –*z*.

Table S5 Selected bond lengths (Å) for **1**/**3**/**4** at 293 K

		1γ phase at 293 K	
Rb(2)–O(3)	2.83(5)	La(1)–O(4)	2.66(2)
La(1)–O(5)	2.65(2)		
		3γ phase at 293 K	
Rb(2)–O(3)	2.836(10)	Nd(1)–O(4)	2.55(3)
Nd(1)–O(5)	2.65(3)		
		4γ phase at 293 K	
Rb(2)–O(3)	2.815(19)	Sm(1)–O(4)	2.50(5)
Ce(1)–O(5)	2.65(4)		

Table S6 The fitting parameters of the Havriliak−Negami equation for **2** at a series of temperatures from 143 to 253 K

T (K)	τ_0 (s)	ε_0	ε_∞	α	β
143	8.9×10^{-4}	3.26	2.54	0.14	1.0
153	3.4×10^{-4}	3.41	2.54	0.16	1.0
163	1.3×10^{-4}	3.59	2.55	0.19	1.0
173	5.6×10^{-5}	3.80	2.55	0.21	1.0
183	2.6×10^{-5}	4.03	2.56	0.23	1.0
193	1.2×10^{-5}	4.24	2.57	0.23	1.0
203	5.9×10^{-6}	4.47	2.60	0.22	1.0
213	3.3×10^{-6}	4.70	2.60	0.17	0.89
223	2.3×10^{-6}	4.89	2.60	0.12	0.78
233	1.5×10^{-6}	5.11	2.60	0.09	0.70
243	9.0×10^{-7}	5.41	2.60	0.05	0.63
253	5.2×10^{-7}	5.74	2.61	0.02	0.58

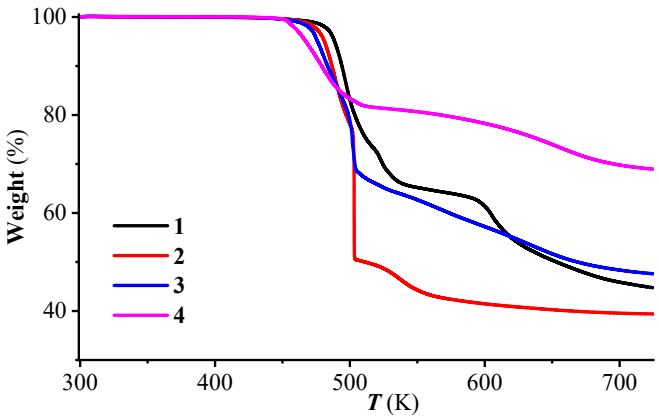

Fig. S1 TGA curves of **1-4**.

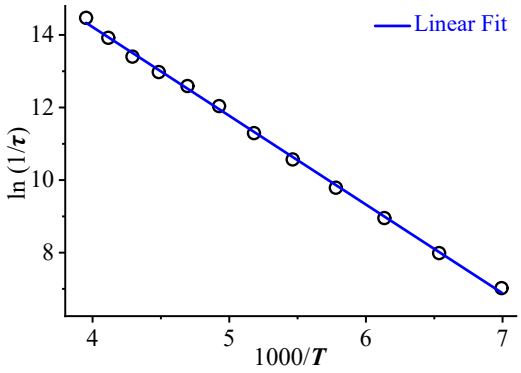

Fig. S2 Arrhenius plots of the relaxation time τ as a function of inverse temperature for **2**.

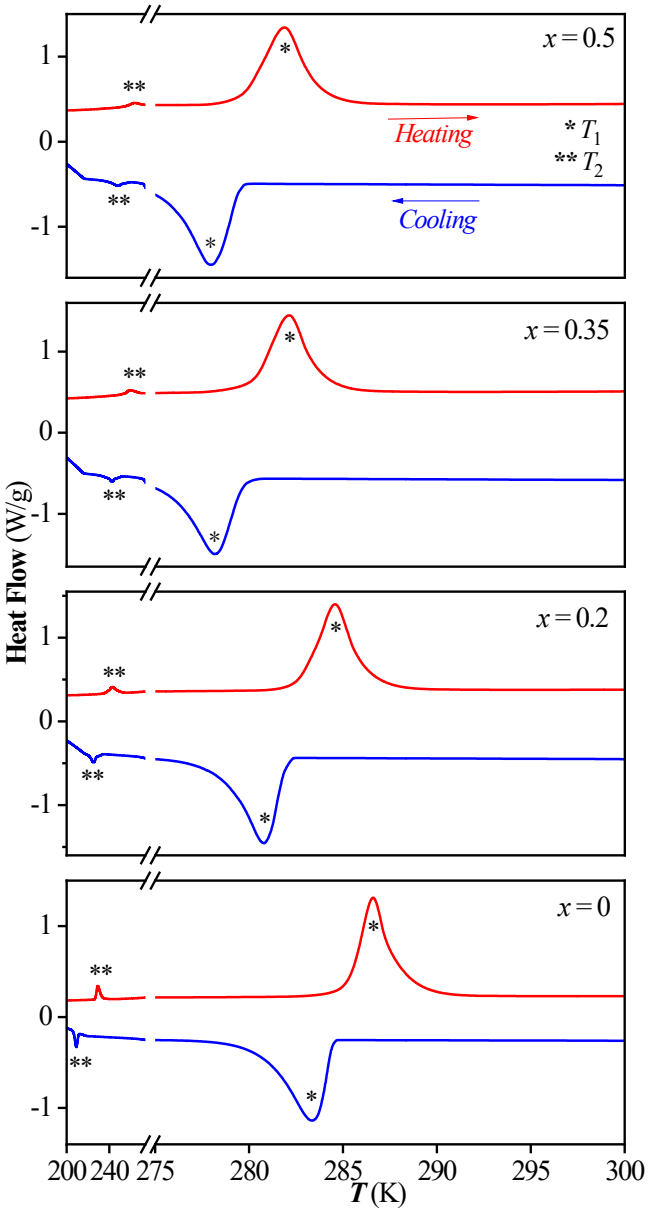

Fig. S3 DSC measurement of (i-PrNHMe$_2$)$_2$[Rb(La$_x$Nd$_{1-x}$)(NO$_3$)$_6$] in a heating–cooling cycle.

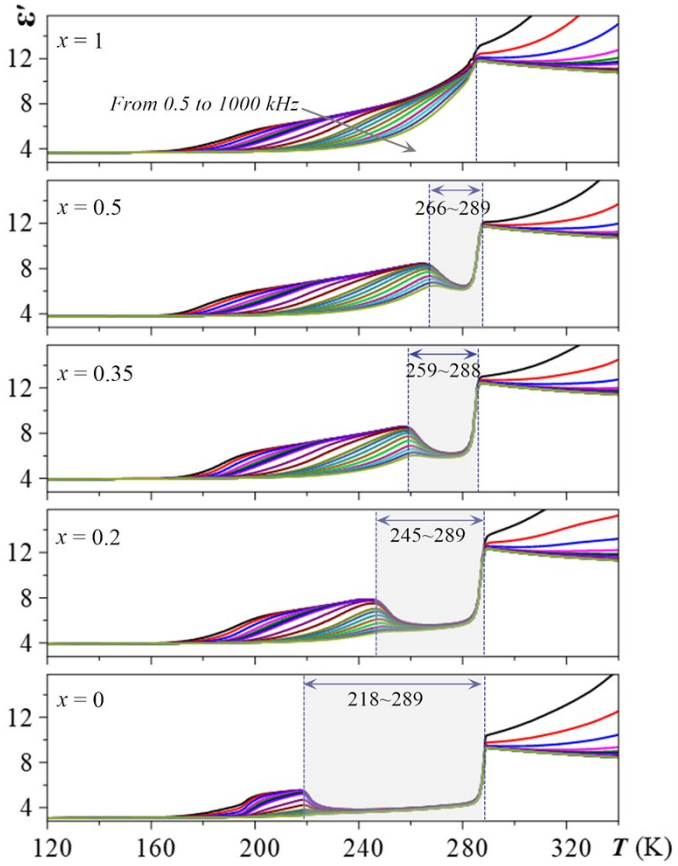

Fig. S4 Comparison of the temperature-dependent multiple dielectric switches of **1**/**3** and their solid solutions (*i*-PrNHMe$_2$)$_2$[Rb(La$_x$Nd$_{1-x}$)(NO$_3$)$_6$] at various ac frequencies. For display detail, see Fig. 3.

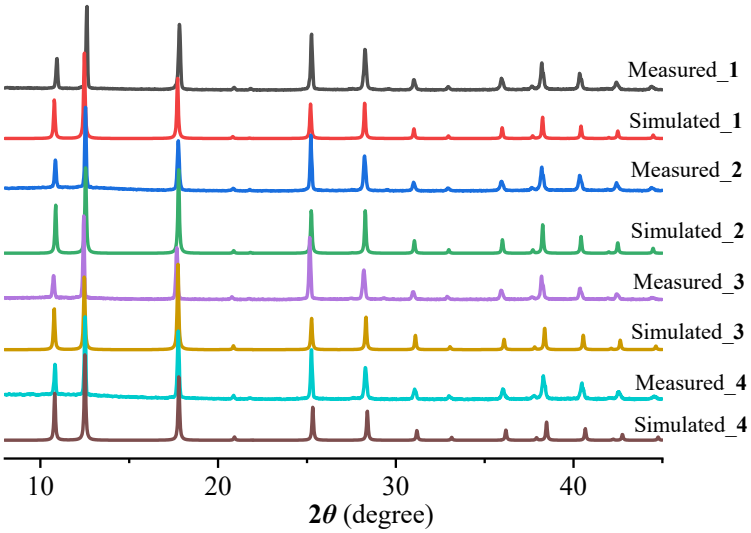

Fig. S5 Simulated and experimental PXRD patterns for **1**-**4** at room temperature.

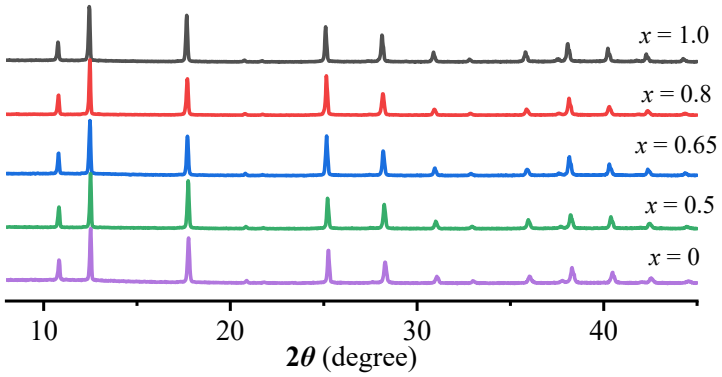

Fig. S6 Comparison of the experimental PXRD patterns of (*i*-PrNHMe$_2$)$_2$[Rb(La$_x$Nd$_{1-x}$)(NO$_3$)$_6$] at room temperature.

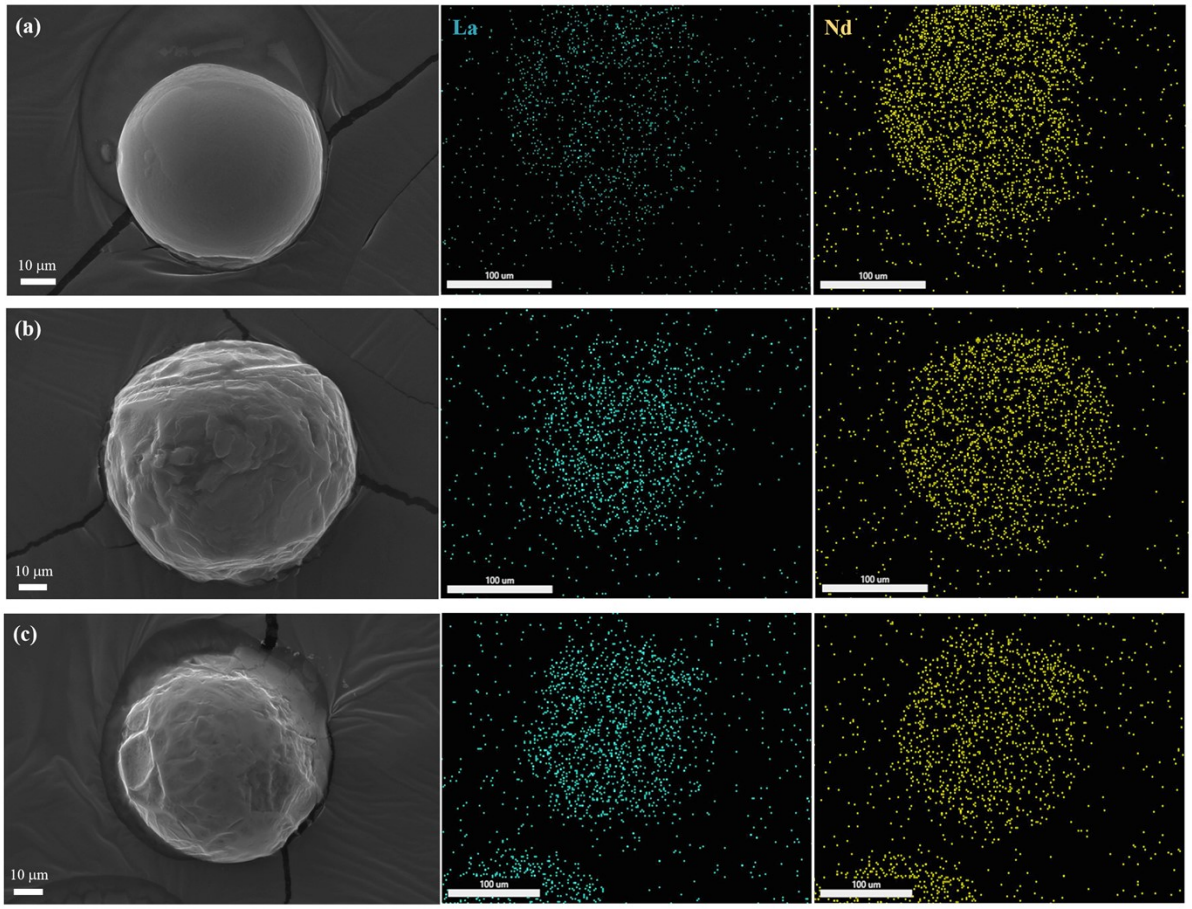

Fig. S7 SEM images and corresponding EDS elemental mapping of La/Nd in the molecular solid solutions (*i*-PrNHMe$_2$)$_2$[Rb(La$_x$Nd$_{1-x}$)(NO$_3$)$_6$], where x = 0.2 (a), 0.35 (b) and 0.5 (c), respectively.

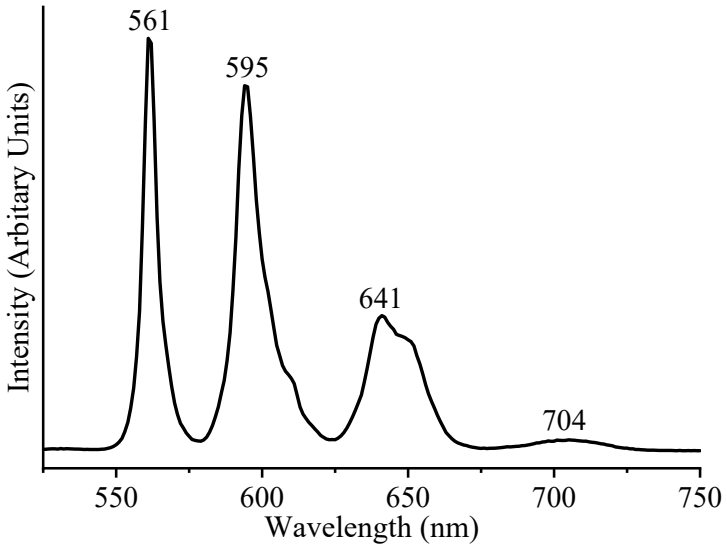

Fig. S8 Solid-state emission spectrum of **4**.